DOI 10.5162/sensor2017/A3.4

# Biosensor based on a split-ring resonator

*T. Reinecke[1], J.-G. Walter[2], T. Kobelt[1], A. Ahrens[1], T. Scheper[2], S. Zimmermann[1]*
*[1]Leibniz Universität Hannover, Inst. of Electrical Engineering and Measurement Technology, Department of Sensors and Measurement Technology, Appelstr. 9A, 30167 Hannover, Germany*
*[2]Institute of Technical Chemistry, Leibniz Universität Hannover, Callinstr. 5, 30167 Hannover, Germany*
*e-mail: reinecke@geml.uni-hannover.de*

**Abstract:**
Split-ring resonators are electrical circuits, which enable highly sensitive readout of split capacity changes via a measurement of shift of the resonance frequency. Thus, functionalization of the split allows the development of biosensors, where selective molecular binding causes a change in permittivity and therefore a change in split capacity. In this work, we present a systematic study of the relevant parameters of a split-ring resonator, verified by electromagnetic simulations and measurements with different sensor topologies. Subsequently, the split of a resonator is functionalized with aptamers and the sensor response is investigated. Here, introducing the target protein results in a shift of the resonance frequency caused by a permittivity change due to aptamer-mediated protein binding, which allows selective detection of the target protein.

**Key words:** Split-ring resonator, selective molecular binding, label-free biosensor, permittivity measurement, aptamers.

## Introduction

Split-ring resonators originate from the field of metamaterials, as they can exhibit effects like negative permittivity and permeability [1]. However, in recent years, there is an increasing use of split ring resonators in sensor and measuring technology, as they allow highly sensitive detection of changes in the polarizability (permittivity) of a material via the detection of a shift of the resonance frequency. Split ring resonators are employed in a broad field of applications [2]. There are systems described in literature, e.g. for dielectric characterization of liquids [3] or analysis of organic tissues [4]. Furthermore, they are found useful for measuring physical values like distance and rotation [5]. Another field of application is material testing for the detection of cracks in metal [6].

Additionally, there are already some biosensors based on split-ring resonators described in literature. In [7] they are used for the detection of Biotin and Streptavidin binding, in [8] for the detection of prostate-specific antigen and in [9] for the detection of Immunoglobin. Furthermore, observation of DNA hybridization is reported in [10].

However, all described resonator structures differ significantly, e.g. in size, shape and used materials, what makes comparison of sensor performance difficult. Thus, the aim of this work is to provide parametric studies based on simulations and measurements, to realize a split-ring resonator exhibiting maximum sensitivity. Subsequently, preliminary results of a first aptamer functionalized split-ring resonator for the label-free detection of C-reactive protein are presented.

## Fundamentals

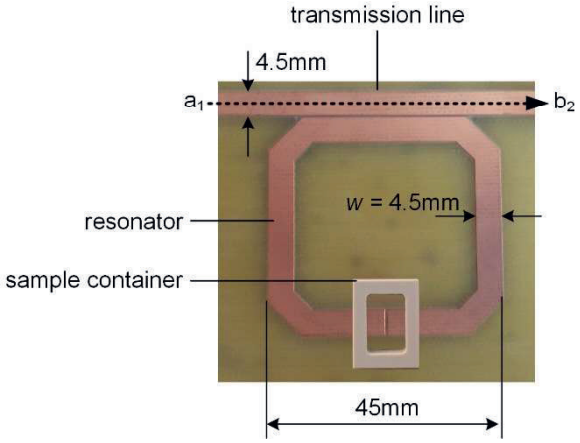


*Figure 1: PCB with split-ring resonator.*

Fig. 1 shows the basic structure of a split ring resonator. The used PCB is a 2.8 mm thick FR4 substrate with a ground plane on the backside. The structure on top layer consists of a transmission line with a width of 4.5 mm leading

to a wave impedance of 50 Ω. Furthermore, a square resonator structure with an edge length of 45 mm is located in a small distance of 300 µm. (In a previous work, the square structure was found to be superior to a round structure, as it leads to a better coupling between resonator and transmission line, combined with a high Q-factor.) Opposite to the transmission line, there is a split in the resonator structure with a sample container placed on top of it.

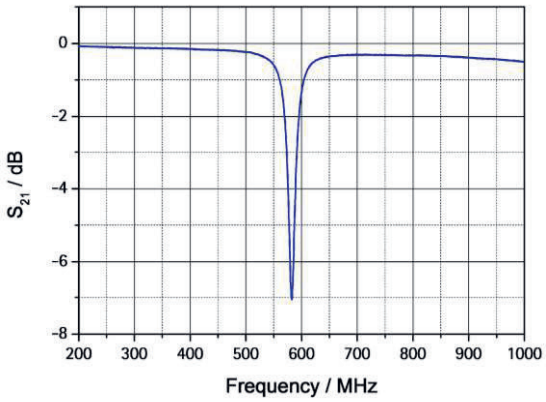


*Figure 2: Transmission measurement of the unloaded split-ring resonator.*

The split-ring resonator is characterized via a transmission measurement ($S_{21} = b_2 / a_1$), i.e. the amplitude ratio of the received wave $b_2$ and the transmitted wave $a_1$. The $S_{21}$ in dependency of the frequency for the depicted resonator loaded with air is shown in Fig. 2. Hereby, the resonance frequency is found at the lowest $S_{21}$ value.

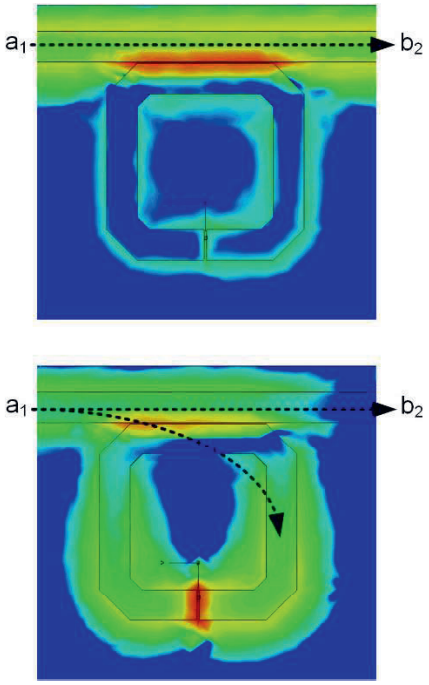


*Figure 3: CST Microwave Studio simulation of the split-ring resonator outside resonance (top) and in resonance (bottom).*

The electromagnetic behavior of the resonator can be visualized via CST simulations as depicted in Fig. 3. Outside of resonance, the resonator structure is virtually field free and thus, all power is transmitted from transmitter to receiver ($a_1 = b_2$). However, in resonance, the wave couples into the resonator structure, where a standing wave is formed. Therefore, there is a high field strength in the ring, especially in the split, and thus power transmission from transmitter to receiver is drastically diminished ($a_1 >> b_2$).

The resonance frequency partly depends on the circumference of the resonator, while a bigger circumference leads to a lower resonance frequency and furthermore, the resonance frequency is determined by the capacity of the split. The influence of the capacity on the resonance frequency can be qualitatively explained with the same mechanisms leading to an extension of the electrical length of half-wave dipoles due to hat-capacitances in antenna technology.

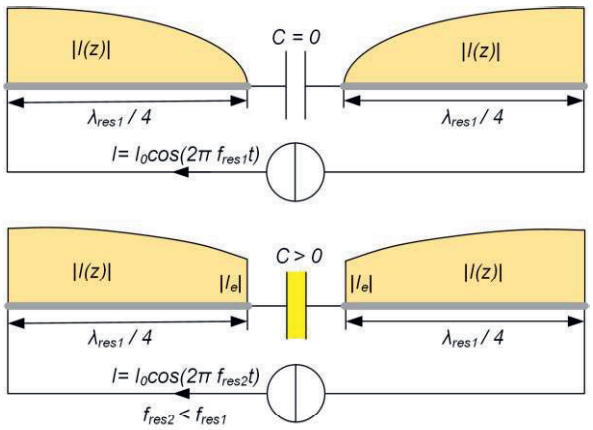


*Figure 4: Current distribution in the resonator structure in resonance for a hypothetical split capacity C = 0 (top) and C > 0 (bottom).*

Figure 4 (top) shows the unwrapped resonator structure with the coupling between transmission line and resonator modeled as current source. In this hypothetical case, the split capacity is *C = 0*. Therefore, the boundary condition for the current distribution of the standing wave on the resonator is *I = 0* at the end of the open sides of the line (position of the split). In this case the half wave length of the resonance frequency equals the circumference of the resonator, here $\lambda_{res1}/2$ = 180 mm and thus the resonance wave length is $\lambda_{res1}$ = 360 mm.

However, when adding a split capacity *C > 0* to the open end of the line, the capacitor is charged with a charge Q and the current at the split becomes $|I| = |I_e| > 0$, with $|I_e| \sim Q$ or $|I_e| \sim C$, respectively. As shown in Figure 5, the capacity at the end of the line, acts like an additional piece

of line, with a length of $\Delta l$, leading to an extension of the electrical length of the resonator. Therefore, the resonance wave length increases ($\lambda_{res2} = \lambda_{res1} + 4\Delta l$) and the resonance frequency decreases to $f_{res} = v / \lambda_{res2}$ respectively. Here $v$ is the propagation velocity of the electromagnetic wave.

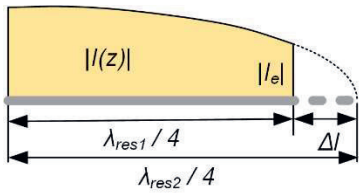


*Figure 5: A capacitive load leads to an extension of the electrical length of the resonator.*

For $\Delta l << \lambda_{res2}$ a simple quantitative description of the dependency between the extension of the electrical length $\Delta l$ and the split capacity $C$ can be found by equalizing the impedance of the split capacity with the input impedance of an open line (stub) of length $\Delta l$:

$$\frac{1}{j\omega C} = -jZ_L \cot\left(\frac{\omega \Delta l}{v}\right). \qquad (1)$$

Using the small-angle approximation, eqn. (1) can be simplified to

$$\Delta l = Z_L v C = Z_L v C_0 \cdot \varepsilon_{r,sample}. \qquad (2)$$

Here, $Z_L$ is the wave impedance of the resonator structure, $C_0$ the capacity of the resonator in air and $\varepsilon_{r,sample}$ the relative permittivity of the material in the sample container. Note, that eqn. (2) is only valid for very small $\Delta l$, which may not be given for the described application. However, the linear approximation in eqn. (2) allows an identification of the parameters responsible for the shift of resonance frequency in dependency of the sample permittivity $\varepsilon_{r,sample}$, which in turn allows a target-oriented optimization process. The exact calculation of the dependency of $f_{res}$ from $\varepsilon_{r,sample}$ is omitted here for reasons of clarity and will be published in a future work.

From eqn. (2) it can be seen, that the sensitivity $S = \Delta l / \varepsilon_{r,sample}$ depends on the split capacity, the wave impedance and the propagation velocity. In the next section, a systematic study of these parameters is performed in order to increase the sensitivity of the setup.

**Setup optimization**

The propagation velocity only depends on the speed of light $c_0$ and the effective permittivity $\varepsilon_{eff}$, which in term is a superposition of the relative substrate permittivity ($\varepsilon_{r,FR4} = 4.1$) and the relative permittivity of air ($\varepsilon_{r,Air} = 1$):

$$v = \frac{c_0}{\sqrt{\varepsilon_{eff}}}. \qquad (3)$$

In order to increase the sensitivity, $v$ has to be increased, which is only possible by decreasing the effective permittivity and thus decreasing the relative permittivity of the substrate. As $\varepsilon_{r,FR4}$ has already a low value, the propagation velocity is not a parameter with broad potential for optimization. Therefore, this section concentrates on $Z_L$ and $C_0$ for increasing sensitivity.

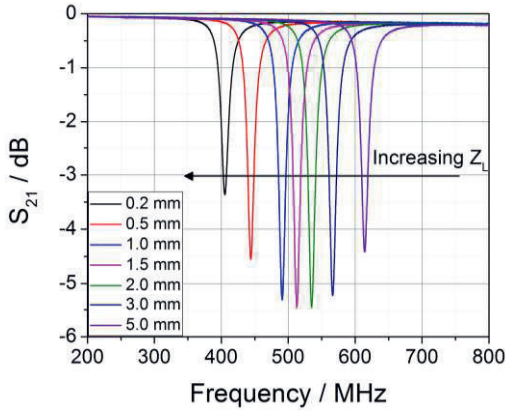


*Figure 6: Measurement results for unloaded resonators with different wave impedances of the resonator structure.*

The wave impedance is in inverse proportion to the conductor width of the resonator structure ($Z_L \sim 1/w$). Figure 6 depicts the $S_{21}$ in dependency of the frequency for resonators with decreasing $w$ and therefore increasing $Z_L$ of the square resonator structure. The width of the transmission line is kept constant at 4.5 mm for all measurements. As predicted by eqn. (2), an increasing $Z_L$ leads to a decreasing resonance frequency. However, a $w < 1.5$ mm leads to a massive deterioration of the coupling between transmission line and resonator structure, as the minimum $S_{21}$ becomes smaller. Therefore, the optimum width of the resonator structure is found at $w \approx 2.0$ mm.

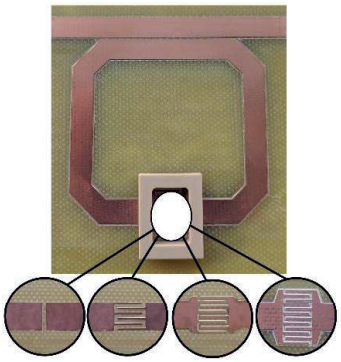

*Figure 7: Split-ring resonator with different split capacities.*

In the next step, the influence of an increasing split capacity $C_0$ on the sensitivity $S$ is investigated. Figure 7 shows the split-ring resonator with different split capacities. To increase $C_0$, interdigital structures are used, instead of a single split. The number of interdigital fingers is gradually increased from 3 per side to six per side. The fingers have a length of $l$ = 5 mm, a width of $w_f$ = 500 µm and the space between the fingers is s = 500 µm.

To investigate the effect on the sensitivity, mixtures of isopropanol ($\varepsilon'_{r,i}$ = 9) with an increasing content of deionized water ($\varepsilon'_{r,w}$ = 80) are filled in the sample container, leading to a sample with increasing relative permittivity. The results are shown in Figure 8. Here, the resonance frequencies are normalized to the resonance frequency of the unloaded resonator.

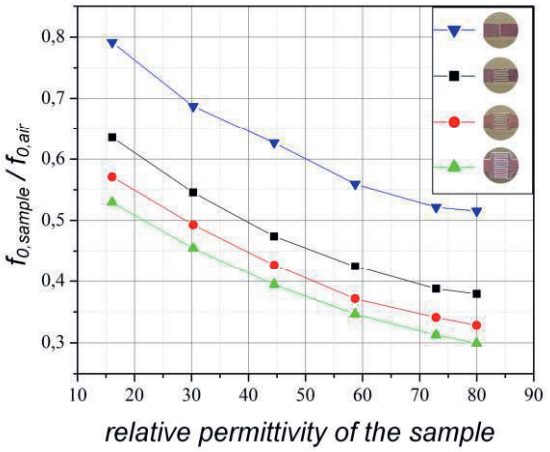


*Figure 8: Measuring an increasing sample permittivity with different split capacities.*

It can be seen that increasing the split capacity leads to a massively increased sensitivity. While the relative frequency shift from unloaded resonator ($\varepsilon_{r,sample}$ = 1) to resonator loaded with deionized water ($\varepsilon_{r,sample}$ = 80) is 50% when using a simple split, the relative frequency shift increases to 70% when using an interdigital structure with 6 fingers.

Another advantage of interdigital structures for the realization of a biosensor becomes apparent by looking at the electrical field in the capacity, depicted in Figure 9. When using a simple split, the penetration depth of the electrical field is relatively high. Therefore, the environment (e.g. permittivity of the sample) has a high influence on the measurement. However, the purpose of a biosensor is to detect binding reactions on the surface of the split capacity and therefore a low penetration depth is preferable in order to increase the influence of the binding reaction and decrease the influence of the environment on the measuring result. Therefore, the 6 finger interdigital structure is superior to the simple split, as the field concentrates around the fingers, see Figure 9 (bottom).

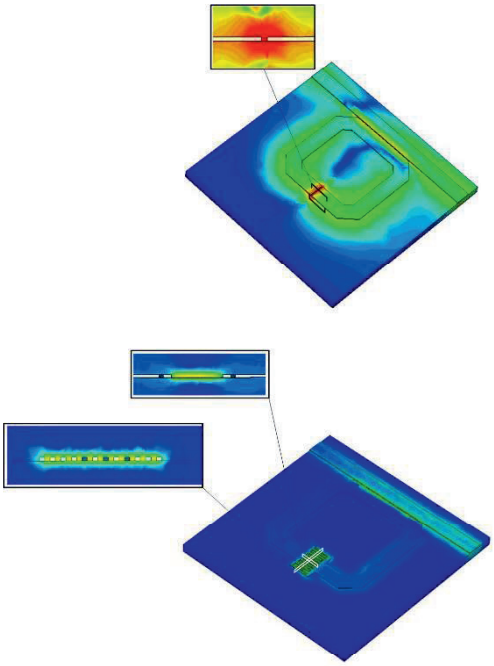

*Figure 9: Electrical field in the cross section of the split capacity for a simple split (top) and interdigital structure (bottom).*

To further decrease the penetration depth and simultaneously increase the capacity, the space between the fingers of the 6 finger structure is gradually decreased from s = 500 µm to s = 150 µm in the final optimization step.

To visualize the effect on the penetration depth, the fluid level in the sample container is gradually increased and the resonance frequency is observed. Due to its' low surface tension, this experiment is carried out with dimethyl sulfoxide (DMSO) with a relative permittivity of $\varepsilon_{r,sample}$ = 46,7.

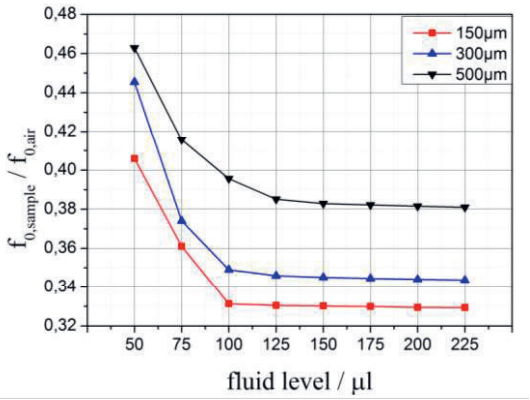


*Figure 10: Decreasing penetration depth via decreasing the space between the fingers of an interdigital structure.*

The results in Figure 10 show that decreasing the space between the fingers leads to an increased split capacity and thus to an increased sensitivity, as there is a higher shift of resonance frequency towards smaller *s*. Furthermore, the penetration depth decreases: While there is still a small frequency shift observable for the resonator with *s* = 500 µm, when increasing the fluid level from 200 µl to 250 µl, the signal already saturates at a fluid level of 100 µl for the resonator with *s* = 150 µm.

The final layout of the split-ring resonator, based on the investigations performed in this section, is depicted in Figure 11.

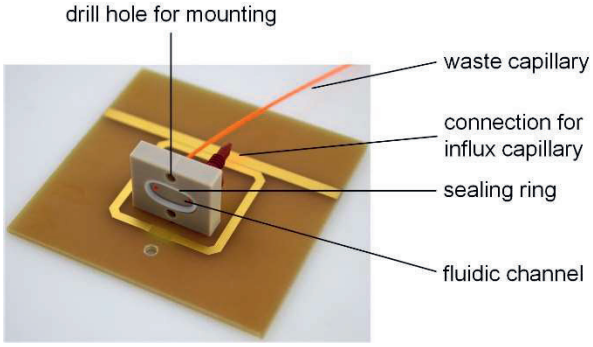


*Figure 11: Final layout of the split-ring resonator.*

The resonator is equipped with a fluidic channel to enable automated measurements with a syringe pump. Furthermore, the conducting areas, especially the split capacity, are chemically coated with gold to enable an immobilization of aptamers as a preliminary test of the split ring resonator as biosensor, which is described in the following section.

**Aptamer based detection of C-reactive protein (CRP) with a split-ring resonator**

In this section, the split capacity is functionalized with aptamers. Aptamers can be considered as artificial alternatives to antibodies, produced via chemical synthesis. Their in-vitro selection process enables the generation of different aptamers selectively binding a huge variety of different target molecules, even toxic or low immunogenic ones. In a first step, the aptamers ability to selectively bind CRP is tested. Therefore, 5´ amino-modified aptamers are spotted on a 3D aldehyde-modified microarray slide (PolyAn,Berlin, Germany) , analog to the procedure described in [11], and subsequently exposed to solutions with different concentrations of fluorescence-labeled CRP to perform quantitative measurements.

Furthermore, the aptamers are exposed to solutions with different concentrations of fluorescence-labeled bovine serum albumin (BSA) to test the selectivity of the aptamers.

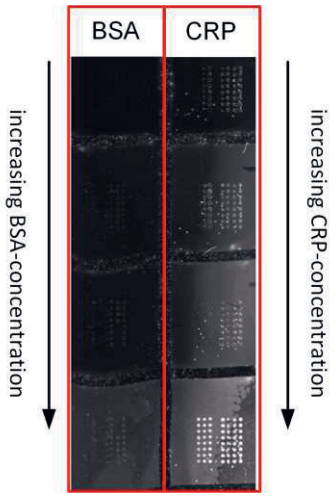


*Figure 12: Optical detection of CRP bound to aptamers.*

The results in Figure 12 show that the fluorescence of the small spots where aptamers are immobilized is increasing when exposed to an increasing concentration of fluorescence-labeled CRP. Therefore, it can be concluded that quantitative measurements of CRP are possible with these aptamers. The test series with fluorescence-labeled BSA shows virtually no response, which leads to the conclusion that the aptamer selectively binds CRP.

Similar to the immobilization procedure described in [12], aptamers are immobilized on the split capacity of a split ring resonator. In parallel, a control resonator is exposed to all chemicals necessary for the immobilization process without finally immobilizing aptamers, to exclude that the sensor response arises from parasitic effects, e.g. an alteration of the capacity, due to reactions with those chemicals. Furthermore, all measurements are carried out after several washing steps, with deionized water in the sample container to eliminate the influence of the permittivity of the solutions containing aptamers and CRP respectively.

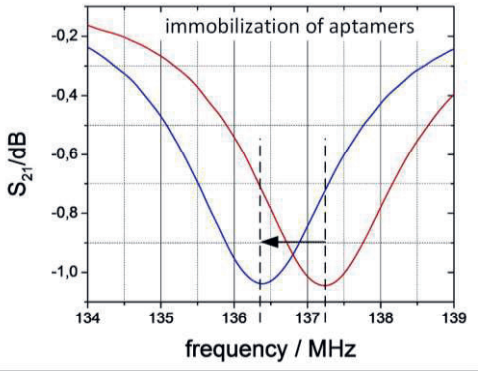


*Figure 13: $S_{21}$ with deionized water as sample before and after immobilization of aptamers.*

Figure 13 shows that the immobilization of aptamers leads to a lower resonance frequency. This can be explained by a good polarizability of the aptamers due to their exposed negative charges. However, the control resonator virtually shows no response after being exposed to the chemicals used for the immobilization process, see Figure 14.

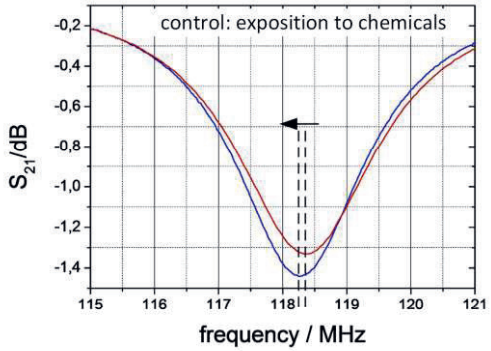


*Figure 14: $S_{21}$ of control resonator with deionized water as sample before and after exposure to immobilization chemicals.*

Subsequently, both split-ring resonators are exposed to a CRP containing solution. The resonator with immobilized aptamers shows a shift of resonance frequency back towards higher frequencies. A sound explanation is that the formerly exposed charges of the aptamers are enclosed and neutralized in the aptamer-CRP binding complex and therefore, the polarizability is massively decreased. Another factor for a decreased polarizability can be the significantly higher mass of the aptamer-CRP binding complex, compared to the unbound aptamer.

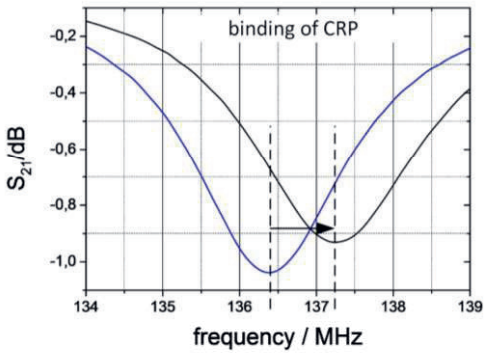


*Figure 15: $S_{21}$ with deionized water as sample before and after binding of CRP.*

The control sensor shows an inverse behavior: The resonance frequency increases after exposure to CRP. This can be caused by binding CRP on the gold surface, leading to an increase in split capacity.

However, the presented results show that aptamer functionalized split ring resonators can be used as biosensors, as the small changes in split capacity due to binding reactions on the gold surface can be detected via the highly sensitive detection of shifts in resonance frequency.

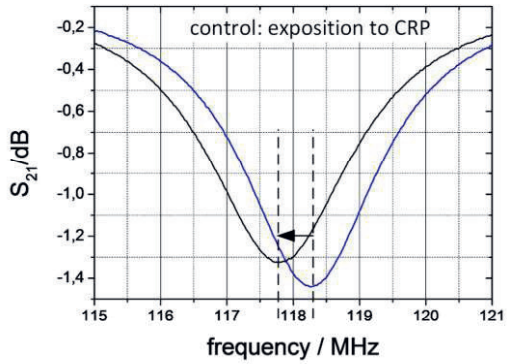


*Figure 16: $S_{21}$ with deionized water as sample before and after exposition to CRP.*

## Conclusion

In this work we presented a systematic investigation of a split-ring resonator for application as biosensor. The parameters responsible for the sensitivity of the setup where determined based on theoretical considerations. Based on these parameters, the resonator structure was optimized. Subsequently, a split ring resonator was functionalized with aptamers and a selective detection of CRP could be shown. In future work, the immobilization process will be improved in order to gain higher sensor responses. Furthermore, the optimal resonance frequency for CRP detection needs to be determined. Finally, quantitative measurements will be performed.

## References

[1] Smith, P.,et al., Physical review letters, vol. 84, no. 18, pp. 4184–4187, 2000.
[2] M. Schueler, et al.," IEEE Microwave, vol. 13, no. 2, pp. 57–68, 2012.
[3] A. Ebrahimi, et al., IEEE Sensors J., vol. 14, no. 5, pp. 1345–1351, 2014.
[4] M. Puentes, et al., 2011 IEEE/MTT-S International Microwave Symposium - MTT 2011, pp. 1–4.
[5] J. Naqui, et al., Sensors, vol. 11, no. 8, pp. 7545–7553, 2011.
[6] A. Albishi et al., Sensors, vol. 14, no. 10, pp. 19354–19370, 2014.
[7] H.-J. Lee et al., Appl. Phys. Lett., vol. 92, no. 25, p. 254103, 2008.
[8] H.-J. Lee et al., Sensors and Actuators B: Chemical, vol. 169, pp. 26–31, 2012.
[9] K. Jaruwongrungsee et al., Procedia Engineering, vol. 120, pp. 163–166, 2015.
[10] H.-J. Lee, et al., Journal of Applied Physics, vol. 108, no. 1, pp. 14908, 2010.
[11] A. Heilkenbrinker, et al., Analytical Chemistry, vol. 87 no. 1, pp. 677-685, 2015
[12] F-C Loo, et al., Sensors and Actuators B, vol. 198, pp. 416–423, 2014